Acta Astronautica 208 (2023) 74–81

Contents lists available at ScienceDirect

Acta Astronautica

journal homepage: www.elsevier.com/locate/actaastro

Illumination conditions near the Moon's south pole: Implication for a concept design of China's Chang'E−7 lunar polar exploration

Guangfei Wei [a,b], Xiongyao Li [c,b], Weiwei Zhang [d,*], Ye Tian [e], Shengyuan Jiang [d], Chu Wang [f], Jinan Ma [f]

[a] Deep Space Exploration Laboratory, Hefei, 230026, China
[b] Chinese Academy of Sciences, Center for Excellence in Comparative Planetology, Hefei, 232006, China
[c] Center for Lunar and Planetary Sciences, Institute of Geochemistry, Chinese Academy of Sciences, Guiyang, 550081, China
[d] The State Key Laboratory of Robotics and System, Harbin Institute of Technology, Harbin, 150001, China
[e] Light Industry College, Harbin University of Commerce, Harbin, 150028, China
[f] Beijing Institute of Spacecraft System Engineering, Beijing, 100094, China

ARTICLE INFO

Keywords:
Moon
Polar regions
Illumination conditions
Chang'E−7
Mission concept design

ABSTRACT

Volatiles including water on the Moon has been one of the most interesting scientific objects for decades. In this study, we systematically introduced a concept for China's Chang'E−7 (CE-7) lunar polar exploration mission which consists of five elements, the orbiter, lander, rover, and leaper, and one relay satellite. The orbiter will provide a high-resolution image preparing for landing site selection. We also proposed three phases for in-situ investigation after landing. (1) The rover and leaper will jointly investigate the sunlit area; (2) the leaper will explore cold traps; and (3) the leaper will fly back to the sunlit area and continue an extended exploration mission. An experimental penetrator launched by the lander will penetrate permanently shadowed crater walls for water ice detection. Data will be transmitted to Earth through the relay satellite due to the limited Earth visibility. We also calculated the illumination rate within a 15 × 15 km area that partially covers the Shackleton crater at a high spatial resolution of 20 m/pixel during lunar southern summer. Specifically, we compared two potential landing sites with accumulated illumination at different altitude levels, slopes, and distances to the target. We found that one part of the Shackleton crater rim can be a primary landing site for CE-7's both sunlit areas and cold trap explorations.

1. Introduction

Lunar polar regions are one of the favorite exploration targets not only because no sample has yet been returned but also because of the likelihood of cold-trapped volatiles including water ice at permanently shadowed regions (PSRs). Unlike mid-low latitudes, the illumination conditions and thermal environment become complex at both poles due to the small tilt of the lunar rotation axis (1.54°) concerning the ecliptic [1–3]. Full knowledge of the polar illumination conditions including perpetual/seasonal shadows and sunlit areas not only helps to inform scientific interests but also plays a part in engineering design for future polar exploration missions. One effective method of determining the lunar polar illumination conditions and identifying extreme insolation locations is to simulate the time-dependent, particularly seasonal shadows and sunlit areas [4], which is important to the future landing site selection, solar power utilization, and the traverse design.

The most directed approach for retrieving lunar polar illumination conditions is analyzing orbital images for certain areas. Bussey et al. [5] analyzed the lunar polar images obtained from the Clementine mission, however, the short mission lifetime (71 days) limited the investigation of illumination. Based on the long lifespan of the Lunar Reconnaissance Orbiter (LRO), Speyerer and Robinson [6] investigated lunar polar illumination conditions for a period of one year based on 7800 Lunar Reconnaissance Orbiter Camera Wide Angle Camera images. However, the determined one-year illumination cannot be exactly applied to any other period due to the lunar precession, such as a future lunar polar exploration mission.

Compared to image analysis, the illumination conditions can also be simulated using a digital terrain model (DTM) for any period. Based on the Earth-based radar-derived polar topography with 150 m spatial

* Corresponding author.
E-mail address: zweier@hit.edu.cn (W. Zhang).

https://doi.org/10.1016/j.actaastro.2023.03.022
Received 20 September 2022; Received in revised form 7 March 2023; Accepted 17 March 2023
Available online 20 March 2023

resolution and 50 m height resolution, Margot et al. [7] used the ray-tracing method to simulate the illumination conditions at both poles. Noda et al. [8] used the first complete lunar polar topography with a resolution of 470 m derived from the Laser Altimeter (LALT) onboard the Japanese KAGUYA mission and employed the ray-tracing method to simulate illumination conditions over one lunar precession period for both poles. Later, Bussey et al. [9] performed a similar simulation with a slightly improved LALT DTM but at the same resolution.

Based on high-resolution altimetry data obtained by LRO Lunar Orbiter Laser Altimeter (LOLA), Mazarico et al. [10] used the 240 m digital elevation model (DEM) and combined the horizon method to simulate the lunar polar illumination conditions with significantly increased spatial and temporal extent. De Rosa et al. [11] used a similar approach but with a resolution of up to 40 m/pixel to simulate illumination conditions at several specific sites of the lunar south pole for future European Space Agency's lunar lander mission. Based on the geometrically adjusted 20 m/pixel DTM from LOLA, Gläser et al. [12] investigated the illumination conditions of a 20 × 20 km region in detail for future landing missions. Later, Gläser et al. [13] generated a north polar LOLA DTM and improved the south polar LOLA DTMs, and identified a total of six potential exploration sites near both poles based on illumination simulations. They also found that a supposed 2 m structural height of a lander has higher levels of average illumination than that on the ground. Recently, Barker et al. [14] improved the LOLA elevation maps up to 5 m/pixel of four high-priority lunar south pole landing sites, and discussed in detail the effect of surface height uncertainty on illumination conditions.

2. Chang'E−7 mission concept for polar exploration

2.1. Mission concept design

China has announced an unmanned Chang'E−7 (CE-7) mission to explore the Moon's south pole between 2024 and 2026. One of the CE-7's scientific goals is to investigate volatiles in polar regions, especially for water ice at cold traps. Here, we propose a concept of mission design that includes five elements, the orbiter, lander, rover, leaper, and one relay satellite. We also propose an in-situ investigation with three phases after landing. In phase I, the rover and leaper will jointly investigate the sunlit area. In phase II, the leaper will explore the targeted PSRs as well as with an experimental penetrator. In phase III, the leaper will return to the sunlit area and continue the geological investigation under an extended mission. These three phases of in-situ exploration will be introduced in detail in the following context. Note that the mission definition and spacecraft configurations have been accepted but the design of each module is still under development.

The relay satellite. The previous study shows that the visibility of the Earth is an important parameter to determine whether a position is favorable for a landing site [10,12]. In addition, if the landing site is located on the far side of the Moon, communication with Earth cannot be direct either. To minimize the engineering risk but maximize the landing site selection, we propose a relay satellite for communication and data transmission due to the limited Earth visibility. An inclined elliptical lunar orbit with a frozen eccentricity will provide a long period of communication with the mission element during two-thirds of its orbit period. In addition, scientific payloads aboard the satellite can also carry out high-resolution observations of the Earth's magnetotail, radio astrometry, and other exploration missions [15], which weigh a total mass of about 450 kg.

The orbiter. The orbiter also consists of several advanced payloads that can provide high-resolution images of the lunar south pole and spectral analysis of surface composition in the sunlit area [15], which is crucial for landing site selection. For example, an interferometry SAR (InSAR) aboard the orbiter will obtain high-resolution images for the evaluation of landing site selection. This will provide detailed surface information including exposed rocks/boulders, and meter-scale craters for the leaper's landing site selection at permanently shadowed craters. Importantly, the orbiter will also investigate the potential hydrogen/-water distribution at targeted PSRs, which provides detailed information for the leaper's exploration.

The lander. The lander carries two probes, the rover, and the leaper, which are combined during orbiting the Moon. After landing, the lander will explore the surrounding environment using solar power, for example, the lunar seismic activity [15]. In addition, the lander carries an experimental payload, the penetrator, which will be launched to penetrate the regolith at a speed of 100 m/s and to a depth of at least 1 m at the permanently shadowed crater wall. The sensors integrated inside the penetrator can provide additional information such as mechanical, electrical, and thermal properties of the regolith of cold traps, which the leaper cannot reach due to engineering risks. The experimental data of the penetrator will be sent to the relay satellite at X-band directly. The penetrator is designed to be powered by a solid-propellant rocket engine that weighs a total mass of 20 kg with a dimension of 1 m in length and 90 mm in diameter. It is worth noting that the lander is designed for a long-term geological investigation and space environment observations of no less than 8 years.

The rover. The rover will also be released to the lunar surface with the assistance of a transfer mechanism. It is also designed to operate in sunlit areas for a period of 8 years. Fig. 1 illustrates that the rover is equipped with a robotic arm, a short drill, and a microvolume sampler which is mounted at the end of the drill. Thus, the rover can work in two kinds of modes: wide-area multi-point sampling mode and longitudinal multi-point sampling mode. Under the control of the robotic arm, the short auger can drill the regolith at different depths, while the microvolume sampler can collect drilling cuttings at the milligram level. The samples are then transferred to the lunar volatiles meter which is installed inside the rover body for further analysis. Notably, the lunar volatiles meter is newly designed, which can detect H_2, H_2O, CO_2, Ar, NH_3, CH_4, etc. With a mass resolution of <1 AMU, an analysis range of 2–150 AMU, and measurement accuracy of about 1%. In addition, the rover will also be equipped with a suite of instruments, i.e., a Raman spectrometer, a lunar penetrating radar, and a lunar surface magnetometer to investigate the landing site area for mineral composition, subsurface structure, and magnetic field [15]. The mass budget of the rover weighs about 140 kg which consumes less than 200 W. The operation and functionality of the rover are powered by solar energy, which requires 300 Watts for traveling and 270 Watts for drilling. However, the heat preservation of the rover is maintained by atomic power. To accomplish a wide area exploration goal, the rover is capable of traveling with a maximum speed of 200 m/h and a gradeability of 15°. This will provide a basic rule for landing site selection and path planning.

The leaper. The leaper is released from the top of the lander which has two movement modes: jumping and walking. The jumping mode will be enabled by the unsymmetrical dimethylhydrazine-fueled engine, which makes the leaper reach a longer distance (more than 30 km in a round trip) and an interesting target possible, for example, the bottom of the permanently shadowed crater. The walking mode is powered by solar energy. Once landed, the leaper can move by walking legs, which can avoid the engine plume contamination area. Similarly, the leaper will work at cold traps in two modes: wide-area multi-point sampling mode and longitudinal multi-point sampling mode. The total mass budget of the leaper is about 400 kg which includes a ground mapping radar for landing site selection in shadowed craters. As illustrated in Fig. 2, the leaper is equipped with a drilling and sampling device, which is enhanced with rotary and percussive drilling ability to break up potential icy layers/blocks. The leaper can sample and analyze with equipped lunar water molecule analyzer [15] at different locations under walking mode. The water molecule analyzer is also newly designed to detect water signatures at PSRs with an analysis capability of <100 AMU and a high signal-to-noise ratio of 1000. The detection

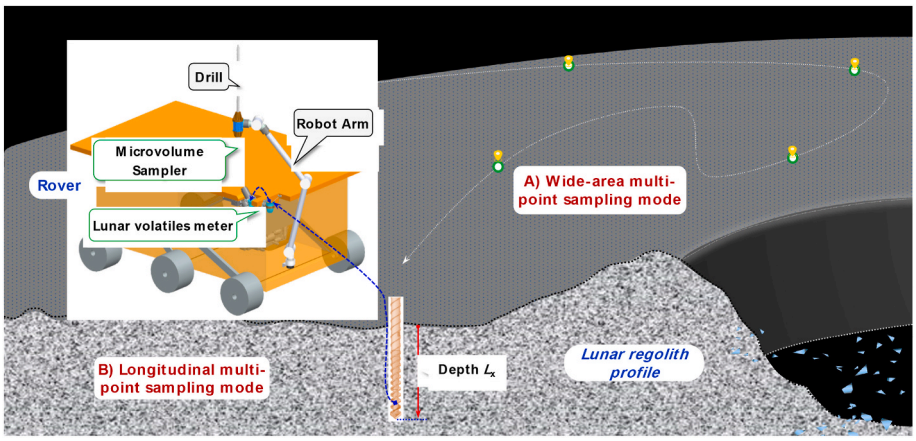

Fig. 1. Illustration of the rover's detection and sampling. L_x indicates the maximum drilling depth. The figure is not drawn to scale.

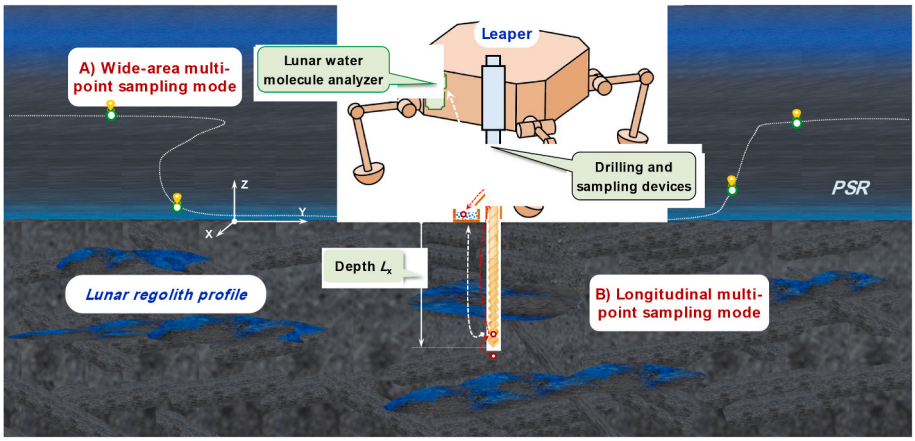

Fig. 2. Illustration of the leaper's detection and sampling. L_x indicates the maximum drilling depth. The figure is not drawn to scale.

limit of the water ice in the drilled sample is 0.1 wt%. Once the sampling mission is completed, the leaper will fly back to the sunlit area and carry out an extended exploration mission. Note that the scientific mission of the leaper is designed for a few months which includes no more than 10 h of operation in cold traps. Considering the limited time of investigation in PSRs and possible extreme topography, the leaper is capable of "walking" at a speed of 12 m/min and climbing a maximum slope of 30°. That is, the leaper can move ~6.5 km within 9 h if not considering sampling time, which is approximate to the size of the Shackleton floor.

2.2. A case study of potential exploration target: shackleton crater

The position with a high illumination rate and lower slope makes it possible to design a long-duration landing mission with sustainable solar power and conventional thermal control systems of the lander and rover [11]. Both optical observations and illumination simulations show that high mountains and crater rims near both polar regions present relatively long continuous lighting environments. These regions can be the primary favored target landing sites of the CE-7 mission, while the illumination conditions at specific locations need to be evaluated based on the planned mission period. Shackleton crater (89.655°S, 129.2°E) is one of the prime targets for future polar exploration not only because of its large area of permanent shadows (232 km^2 [10]) within the crater which can trap volatiles [16], but also its persistent access to solar energy along the rim and/or nearby ridges [6,8]. In addition, it appears to be rough at Shackleton's crater wall on the sub-meter scale but smooth on the crater's bottom [12]. That is, the floor of the Shackleton crater will be an ideal place for the leaper's in-situ exploration. Therefore, regions like the Shackleton crater are of great interest to both scientists and engineers expecting long-term geological investigation and in situ resource utilization of cold-trapped water ice.

The extremely low temperature of PSRs such as the Shackleton crater can cold-trap water molecules once they are distributed and/or deposited by comets, solar wind implantation, and volcanic outgassing [2,17]. Using the reflectance of the lunar surface from LOLA observations, Zuber et al. [16] explain the relatively brighter Shackleton crater floor might be caused by a water ice-bearing 1-μm-thick layer. Based on scattering light in PSRs, Li et al. [18] find direct evidence of exposed water ice at near-infrared spectra at the lunar south pole which also includes the Shackleton crater. Using the pixon image reconstruction technique, Teodoro et al. [19] determined the water equivalent hydrogen to be ~ 0.6 wt% at Shackleton crater. Additionally, the Lunar Crater Observation and Sensing Satellite (LCROSS) experiment has confirmed the abundance of volatiles by analyzing the near-infrared spectra of ejecta plumes at Cabeus crater [20]. Therefore, it is reasonable to drill samples at the bottom of the Shackleton crater for investigating water ice and other volatiles. Here, we take the Shackleton crater as an exploration target to illustrate landing site selection based on our mission concept design and evaluation of illumination conditions.

3. Data and method

The LOLA altimeter is one of seven scientific instruments aboard LRO that was commissioned on July 13, 2009. LOLA is designed to measure the shape of the Moon with a multi-beam and high-repetition-rate laser altimeter system [21]. Digital elevation models (DEMs) of the polar

regions have been constructed based on the unprecedented spatial resolution which is about 10 m in the along-track direction at the nominal 50 km near-circular mapping orbit [10,14]. In this study, a 15 × 15 km region near the lunar south pole that partially covers the Shackleton crater is investigated by calculating illumination conditions with a 20 m/pixel DEM map that is derived from LOLA data (http://imbrium.mit.edu/). The area and resolution chosen here are a compromise between computation time and spatial accuracy. However, it is sufficient to simulate the actual lighting conditions accurately for a relatively long-time scale. It is worth noting that the illumination conditions of the 20 m scale are still much coarser than the apparent footprint of the surface mission element. The specific landing site in regions of interest can be further determined from high-resolution images of the orbiter, which is beyond the scope of this study.

Numerical simulation of polar illumination conditions has been widely used to investigate the Moon's poles with different digital terrain models [5,7,8,10]. Some researchers preferred the ray-tracing method [5,8,9] due to the accuracy of simulation, while this calculation has to be repeated each time step. Therefore, the ray-tracing method is well-adapted for short periods but is very time-consuming on a large area and long timescale, whereas, the horizon technique only costs a long computation time once for retrieving the horizon at each pixel and stores the maximum elevation in different azimuth direction [10–13]. With a little sacrifice of accuracy concerning the ray-tracing method, the computation speed has been improved significantly.

In this study, we employ the horizon method that is similar to those previously described by Mazarico et al. [10] and Gläser et al. [12]. The Navigation and Ancillary Information Facility [22] (NAIF) was developed by NASA to provide assistance and information about the space-borne instrument and planetary mission modeling. Here, we use the NAIF/SPICE library and kernels to compute the Sun-Moon geometry. Then we combined the LOLA topography to characterize the illumination conditions. We conducted the simulation with a high temporal resolution of 1 h to identify the most illuminated regions within the study area. Additionally, the position of the Sun and its apparent radius are updated at each time step. The azimuth step of each pixel is 0.5° which will create 720 of the highest elevations after computing all the elevations along the line of sight. Specifically, the time step, 1 h corresponds to the Sun's angular diameter and the azimuth step during which the Moon rotates about 0.5° [12]. Note that both the distances measured in the map and the height differences are corrected for the DEM polar stereo projection distortion. Given a certain time and/or period, one can calculate the solar elevation at each pixel and compare the corresponding horizon to decide whether it is illuminated or not. By treating the Sun as an apparent disk rather than a point source, the illumination map is created from the fraction of the visible solar disk at each pixel.

4. Results

4.1. A case study of the proposed CE-7 mission period

Lunar polar illumination conditions can be different at different seasons due to the precession cycle [1,3]. Although the average illumination rate of 18.6 years at both poles has been investigated, the illumination conditions for a specific lunar polar exploration mission within a period can be different. That is, the selection of the best landing site for the CE-7 mission could be different when taking into account different periods.

The Diviner measurements show that the temperature within PSRs presents a dominant seasonal variation during the Moon's draconic year [3]. Such variation in the thermal environment is dramatically controlled by illumination conditions. Here, we define the lunar season of each pole simply by subsolar latitude that is above or below the equator. Fig. 3a shows the subsolar latitude variation within the time span of 2024–2025. The full range of southern winter (blue shaded area) and summer (red shaded area) within 2024 start on April 4 and September 28, respectively. Considering the efficiency of power utilization and thermal control system, we calculate the accumulated illumination over the period between September 28, 2024, and March 17, 2025. Additionally, the Sun-Moon distance also presents a variation due to the Moon's rotation and revolution (Fig. 3b), which controls the Sun's apparent radius and irradiance that arrives on the lunar surface.

Fig. 4 shows the illumination rate at a surface level within a 15 × 15 km area at a spatial resolution of 20 m/pixel that is near the lunar south pole and partially covers the Shackleton crater. No areas are identified to

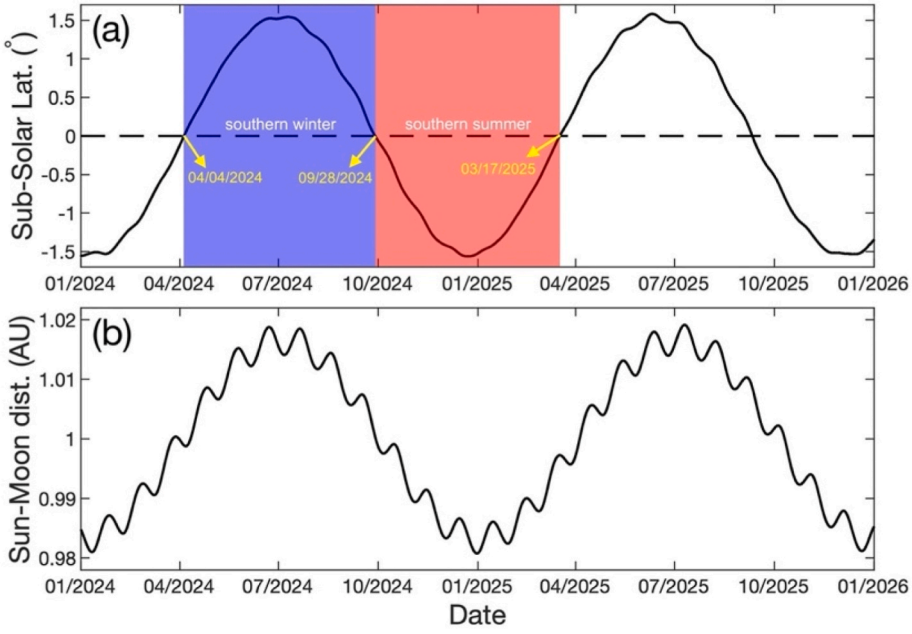

Fig. 3. Variation of lunar orbital parameters in the years 2024 and 2025. (a) Is the subsolar latitude which indicates the seasonal variation of the Moon. The blue and red shaded areas indicate the full range of southern winter and summer start in 2024, respectively. The dashed line indicates the lunar equator. (b) Is the Sun-Moon distance in AU. (For interpretation of the references to colour in this figure legend, the reader is referred to the Web version of this article.)

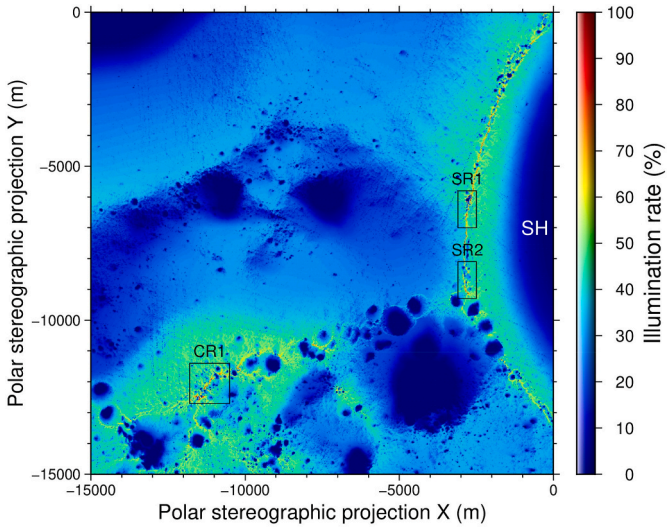

Fig. 4. The average illumination rate of the study area near the Moon's south pole between April 4, 2024, and March 17, 2025. The area enclosed by black boxes (SR1, SR2, and CR1) is a potential landing site area. The map is created in polar stereographic projection and the coordinate (0,0) indicates the lunar south pole. "SH" represents the Shackleton crater.

receive constant sunlight during the considered period. As expected from previous studies [10–12], the Shackleton crater rim and its surrounding highest terrains are found to be the most illuminated areas. But these regions are characterized by different topography and surrounding perpetual and/or seasonal shadowed craters. Since the landing site selection and/or traverse design are crucially dependent on the scientific goals and engineering capabilities, other factors such as surface slopes, distance to exploration targets should be considered as well as illumination conditions.

4.2. *Illumination conditions at potential landing sites*

In this part, we first select three potential landing sites (black boxes in Fig. 4) with relatively high illumination rates that have also been investigated by previous work [11,12]: two Shackleton Rim (SR1 and SR2) and one "Connecting Ridge" (CR1) between Shackleton and de Gelarche craters. Note that the area of SR2 investigated here is larger than in previous work [12] but is the same as SR1, which is convenient for comparison. Then, we filter these areas by restricting surface slopes by considering engineering safety. Here, we focus on different periods by considering the illumination rate, surface slope, and illumination conditions at different heights above the surface. These factors are important for mission design studies, in particular for the identification of optimal landing sites [23], rover traverse planning, and solar array height and location [10,11]. In addition, we also evaluate the distance between the landing sites and the center of the Shackleton crater to compare the capability requirement of the leaper and penetrator.

The surface area of favorable landing zones should be evaluated to provide accurate constraints on landing site selections. As shown in Figs. 4 and 5a,d, regions of these three landing sites with illumination rates greater than 60% are distributed in lines and clusters that are

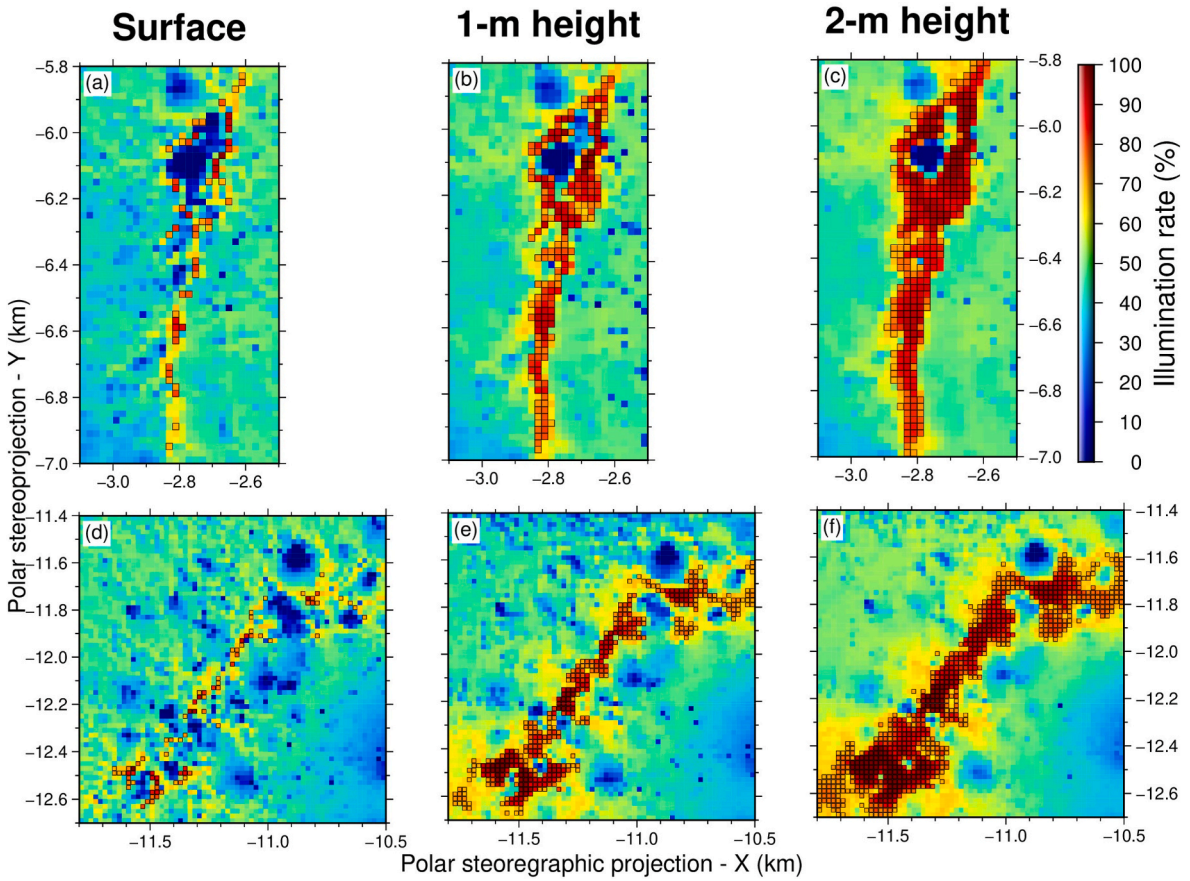

Fig. 5. Comparison of illumination rate at two potential landing sites. (a), (b) and (c) are SR1 landing site areas with the center coordination 156.3709°W, 89.7692°S. (d), (e) and (f) are CR1 landing site areas with the center coordination 137.2214°W, 89.4586°S. The left, middle and right columns indicate illumination rate at the surface, 1 m and 2 m height above the surface, respectively. The pixel enclosed with black boxes indicates an illumination rate greater than 70% and a surface slope less than 10°.

controlled by topographic relief. Considering a higher illumination rate of >70% and a small slope of <10° for engineering safety, the potential landing site in the number of pixels is significantly reduced and the region becomes discontinuous. Specifically, the landing site SR2 only has a total area of 10,400 m^2 (26 pixels) though it has an average illumination rate of 77.0% with the highest value, 96%, and is closer to the floor of the Shackleton crater. Comparatively, SR1 (Fig. 5a) and CR1 (Fig. 5d) present a larger area of 22,000 m^2 and 25,600 m^2, and an average illumination rate of 79.7% and 77.7%, respectively. The area of the two landing sites is mainly discontinuous but with partial clusters (enclosed with black boxes) along the rim and/or ridge. Therefore, in the next paragraph, we will evaluate and compare SR1 and CR1 in detail for landing site selection.

Considering the height of an observer, we evaluate the illumination conditions for a solar panel on a rover with a height of 1 m above the surface. As shown in the middle column of Fig. 5 and Table 1, both the total area and average illumination rate of the two landing sites (pixels enclosed by black boxes) increase dramatically compared to the surface level (left column). Typically, both SR1 (Fig. 5b) and CR1 (Fig. 5e) become mainly continuous and form an elongated area along rims and ridges. We also evaluate the illumination rate at an altitude of 2 m above the surface (right column of Fig. 5) for a solar panel on a stationary lander. It can be seen that both the average illuminate rate and landing site area at SR1 and CR1 increase substantially compared to the surface and 1 m level. Both landing site areas of SR1 and CR1 are completely continuous along the rims and/or ridges. But the CR1 presents a larger cluster of landing site areas than that of SR1. It is worth noting that the CR1 has a relatively ~1.6 times larger total area of the favorable landing site at the surface level than SR1 and a relatively smaller illumination rate than SR1 at all levels. However, the total area of CR1 at 1-m and 2-m level increase more rapidly than that of SR1 and form larger clusters.

5. Discussion

5.1. Potential landing site selection

Based on our concept of the CE-7 lunar polar exploration mission, the leaper will fly to cold traps to explore water ice by drilling samples. Compared to rover exploration, the leaper can target great distances without considering the potential hazardousness, for example, exposed rocks, extreme slopes, and darkness during the traverse. Although the Shackleton crater studied here has a large wall slope with an average of 31°, most of the floor is nearly flat, which is a favorable exploration site for the leaper. Furthermore, the leaper moves fast which can reduce exposure time in cryogenic regions, which will lower the engineering risk. Similarly, the range between the lander and target for the penetrator exploration only needs to be considered here. In this part, we compare the average illumination rate, total landing site area, slopes, and distance to the exploration target in detail for landing site selection.

Since SR1 is part of the Shackleton rim, it has the shortest average distance, ~11 km (i.e., about the radius of the crater) to the crater center. However, CR1 has a greater distance than that of SR1 by a factor of ~ 2. This will result in more energy consumption for both the leaper and the penetrator. Considering the altitude of the solar panel on a rover and a lander, the total area of possible landing site (with a basic rule of both average illumination rate >70% and slope <10°) at CR1 increases faster than SR1 but with smaller slopes (Table 1). That is, the large area of the CR1 landing site provides more choices for landing site selection and traverse planning, which in turn could reduce the engineering risks during the landing. But the relatively high illumination rate of SR1 is more favorable for solar power utilization and thermal control system, especially for long-term exploration missions. Based on the above basic rule, we further restrict the landing site selection with the order of (1) distance to the target and (2) illumination area under consideration of the range capability of the leaper and the penetrator. Therefore, it is advantageous to select SR1 as a primary landing site for exploring the Shackleton crater. Alternatively, CR1 is also an interesting landing site because of its large possible landing site area and smoother surface when the distance is not considered.

Table 1
Comparison of total areas (m^2), average illumination rate (r_{ill}, %), and average slope (°) at different landing site areas with illumination rate greater than 0.7 and slope less than 10°.

	SR1			CR1		
Altitude level	Total Area	Avg r_{ill}	Avg slope	Total Area	Avg r_{ill}	Avg slope
Surface	20,400	79.7	3.0	32,000	77.7	2.1
1 m	91,200	82.3	3.6	201,600	80.9	2.7
2 m	146,000	86.4	4.0	383,200	83.4	3.2

5.2. Patterns of illumination rate at potential landing sites

The period of illumination and/or darkness is crucially important for surface operation, such as solar power utilization and thermal control system. Fig. 6a shows a time history of the visible Sun fraction at 2 m height of one potential landing site (X = −2810 m, Y = −6590 m) within SR1 during the lunar south summer between September 28, 2024, and March 17, 2025. The partially visible Sun fraction (0–1) is repeated during the transition between illumination and darkness. Considering the proportion of solar energy to the visible fraction and the efficiency of power utilization, the visible Sun fraction is converted to a binary illumination/darkness pattern (Fig. 6b) by thresholding 0.5 Sun fraction following the work of [11]. The result shows that there is a continuous 57 days of illumination and a maximum period of darkness of about 2 days and a half during the time range. Considering the capacity of the power system of the lander/rover, a short period of darkness can be further excluded to reduce the unfeasibility of short system hibernation times. Fig. 6c and d shows patterns after filtering darkness periods shorter than 13 h and 44 h, respectively. The duration of the longest illumination periods has been increased dramatically to 86 and 97 days. That is, the improvement of the power capacity of the lander/rover operating in darkness can increase the apparent continuous illumination periods for ground operation and investigation. Comparatively, we also computed a time history of the visible Sun fraction at 2 m height of

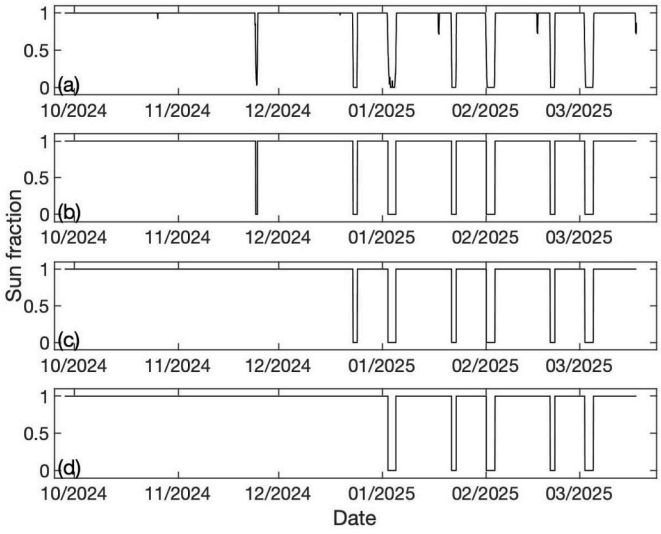

Fig. 6. (a) Variation of visible Sun fraction during lunar southern summer between September 28, 2024, and March 17, 2025, at 2 m height of one potential landing site (X = −2810 m, Y = −6590 m). (b) The pattern of illumination after filtering to 0.5 of Sun fraction. (c) and (d) Patterns after filtering of darkness/shadow periods shorter than 13 h and 44 h, respectively.

another potential landing site (X = −11,570 m, Y = −12,470 m) of CR1. The result shows that it can always receive continuous illumination within the considered time range (~170 days). This will enable surface operation with the longest period of continuous power supply during the investigation. However, this favorite landing site is much farther away than the SR1 concerning the targeted Shackleton floor, which as a result requires more propellant for the leaper's mobility and the launch system of the mission. To meet the scientific goals of water ice exploration at PSRs, a favorite landing site selection should meet the requirement of better illumination conditions and an accessible exploration target.

5.3. Necessity of high-resolution topography/images for the Leaper's target selection

Higher-resolution topography data can provide more surface details including illumination conditions and geomorphology for landing site selection. Currently, the highest resolution of LOLA DEM data covering the lunar south pole we can obtain is 5 m/pixel, which can provide more information about illumination conditions and surface topography than our current study (20 m/pixel). However, the computation of this study area is very time-consuming. Nevertheless, the 5 m/pixel is still coarser than the apparent footprint of surface assets (meter scale). Therefore, we choose the 20 m/pixel data as a compromise between computation time and spatial resolution. As a result, the calculated illumination rate can still provide useful information for possible landing sites and scientific target selection of the CE-7 mission. At present, there is no meter-to-submeter scale topography data covering PSRs, which makes the evaluation of landing site selection and trafficability of the leaper ambiguous. Considering the necessity of obtaining high-resolution topography data and/or images for engineering safety, we also proposed an InSAR that will be equipped for the orbiter to obtain a submeter scale topography and images of the target before landing. Thus, this will provide detailed surface information including slopes, exposed rocks/boulders, and meter-scale craters for the potential landing and exploration sites. Additionally, the leaper is also equipped with a navigation terrain camera and a lighting system, which will help the leaper select a target before landing and avoid obstacles during "walking". Specifically, the leaper can climb a maximum slope of 30°, which makes the leaper's trafficability more flexible. Since this study is focused on computing illumination conditions to provide possible rules of landing site selection for our proposed mission concept. A detailed analysis of the surface topography in the assets scale will be further determined from high-resolution images of the orbiter during the mission, which is beyond the scope of this study.

As mentioned above, the Leaper's specific target of Shackleton's floor is not determined due to the lack of high-resolution topography data. However, the temperature-dependent water ice stability in the targeted area can be evaluated. The Diviner aboard LRO was designed to systematically measure lunar surface temperature globally [24] and the more than 10 years of observations provide diurnal and seasonal constraints on the lunar polar thermal environment [3,25]. Most of the bottom of the Shackleton crater remains at extremely lower temperatures (<110 K) where water molecules can remain stable seasonally. This makes the bottom of the Shackleton crater a candidate for both scientific exploration and in-situ resource utilization. In addition, the theoretical model indicates that temperature cycles of the near-surface at cold traps can drive water molecules downward along thermal gradients to form the thermal stability of buried water ice and "thermally pumped" ice, which is usually stable within a 20 cm depth [26,27]. If water ice is buried in the subsurface, the loss rate is reduced significantly due to the obstruction of the overlying dry regolith and relatively smaller temperature fluctuation, which is favorable for the leaper's sampling.

5.4. Challenges and strategies of the leaper's exploration at PSRs

One of the main scientific objectives of the CE-7 mission is to investigate volatile components including water ice at PSRs. Compared to China's previous successful Chang'E−5 lunar sampling return mission, the sampling mission at cold traps of the leaper we proposed in this study still faces great technical challenges. (1) The extremely low temperature at PSRs is hazardous to the device and sensors of the leaper. (2) The randomly distributed surface water ice makes it difficult for the leaper's landing site selection and traversing within a limited operational time. (3) The ice-bearing regolith presents an extreme mechanical strength with different ice saturation [28], which makes the drilling difficult. (4) The temperature dependence of volatile evaporation could be caused by the heat during the drilling, which is a challenge to microgram-level sampling.

To sample water ice efficiently, we propose a general sampling strategy and manipulation method of the leaper. (1) Pre-judgmental location selection. Using an infrared spectral camera and neutron spectrometer onboard the leaper to characterize the surface before drilling. If there is no hydrogen and/or water signal, the leaper will move to another place. (2) Intelligent drilling. Developing an automatic control system, for example, integrating a dielectric sensor at the front end of the drilling tool to identify soils, rocks, and water ice during the drilling process. (3) Low perturbation sampling. To monitor and adjust the drilling status which might overheat the surrounding materials, a thermal sensor should be integrated into the drilling tool. (4) Real-time drilling data correlation analysis. Combining the temperature, dielectric properties, and mechanical status during drilling for real-time analysis to provide a comprehensive understanding of the sample.

6. Conclusion

Volatiles including water ice cold-trapped in permanently shadowed regions are one of the most interesting scientific topics for lunar polar exploration. In this study, we proposed a general concept for China's future CE-7 lunar polar exploration mission. It consists of four probes, the orbiter, lander, rover, and leaper, and one relay satellite. The orbiter observation can provide a high-resolution image of the sunlit area for landing site selection and investigate hydrogen/water distribution at PSRs for the leaper's exploration planning. The lander not only carries the rover and leaper, but also a penetrator which will be launched to penetrate the permanently shadowed crater wall for water ice detection. The rover and leaper will sample by drilling at the sunlit area and cold traps, respectively. Once the sampling mission has been completed, the leaper will join the rover to continue to explore the sunlit area with an extended mission. All data will be stored and transmitted to Earth through the relay satellite due to the limited Earth visibility.

We also take the Shackleton crater as a study case for our proposed CE-7 mission concept. Based on the high-resolution LOLA DEM, we calculated the accumulated illumination within a 15 × 15 km area during the lunar southern summer between September 28, 2024, and March 17, 2025. No region has been found to receive constant illumination during this period. However, two Shackleton Rim (SR1 and SR2) and one "Connecting Ridge" (CR1) were found to have relatively high illumination rates which were favorable for potential landing sites. Selecting regions with a basic rule of illumination rate >70% and surface slope <10° for engineering safety, the result shows that SR2 received a high average illumination rate but a very small landing site area. Considering the height of an observer at SR1 and CR1, we evaluate the illumination conditions for a solar panel on a rover and a stationary lander with a height of 1 m and 2 m above the surface, respectively (Fig. 5). We found that CR1 not only has a comparable illumination rate with SR1 but also has a very large continuous landing site area with small surface slopes. However, CR1 has a greater distance than that SR1 by a factor of ~ 2 to the center of Shackleton. We also restrict the landing site selection with the order of distance to the target > illumination area

based on our mission concept; we propose to select the SR1 as a primary landing site for exploring Shackleton. In future work, the evaluation of landing site selection can be improved based on more announced details of the CE-7 lunar polar exploration project.

Declaration of competing interest

The authors declare that they have no known competing financial interests or personal relationships that could have appeared to influence the work reported in this paper.

Acknowledgments

We thank the LOLA team produce the high-quality DEM data that was used in this study. The LOLA data is publicly available at http://imbrium.mit.edu/. This work was supported by the National Key Research and Development Program of China (2022YFF0711400), the National Natural Science Foundation of China (42241154, 41931077, 52005136), the Strategic Priority Research Program of CAS (XDB 41000000), and the Science and Technology Program of Guizhou Province (QKHJC-ZK[2023]-476).

References

[1] J.L. Kloos, J.E. Moores, J. Sangha, T.G. Nguyen, N. Schorghofer, The temporal and geographic extent of seasonal cold trapping on the Moon, J. Geophys. Res. Planets. 124 (2019) 1935–1944, https://doi.org/10.1029/2019JE006003.

[2] D.A. Paige, M.A. Siegler, J.A. Zhang, P.O. Hayne, E.J. Foote, K.A. Bennett, A. R. Vasavada, B.T. Greenhagen, J.T. Schofield, D.J. McCleese, M.C. Foote, E. DeJong, B.G. Bills, W. Hartford, B.C. Murray, C.C. Allen, K. Snook, L. A. Soderblom, S. Calcutt, F.W. Taylor, N.E. Bowles, J.L. Bandfield, R. Elphic, R. Ghent, T.D. Glotch, M.B. Wyatt, P.G. Lucey, Diviner lunar radiometer observations of cold traps in the Moon's south polar region, Science 330 (2010) 479–482, https://doi.org/10.1126/science.1187726.

[3] J.-P. Williams, B.T. Greenhagen, D.A. Paige, N. Schorghofer, E. Sefton-Nash, P. O. Hayne, P.G. Lucey, M.A. Siegler, K.M. Aye, Seasonal polar temperatures on the Moon, J. Geophys. Res. Planets. 124 (2019) 2505–2521, https://doi.org/10.1029/2019JE006028.

[4] D.B.J. Bussey, P.G. Lucey, D. Steutel, M.S. Robinson, P.D. Spudis, K.D. Edwards, Permanent shadow in simple craters near the lunar poles: permanent shadow in simple craters near the lunar POLES, Geophys. Res. Lett. 30 (2003), https://doi.org/10.1029/2002GL016180.

[5] D.B.J. Bussey, P.D. Spudis, M.S. Robinson, Illumination conditions at the lunar South Pole, Geophys. Res. Lett. 26 (1999) 1187–1190, https://doi.org/10.1029/1999GL900213.

[6] E.J. Speyerer, M.S. Robinson, Persistently illuminated regions at the lunar poles: ideal sites for future exploration, Icarus 222 (2013) 122–136, https://doi.org/10.1016/j.icarus.2012.10.010.

[7] J.L. Margot, Topography of the lunar Poles from radar interferometry: a survey of cold trap locations, Science 284 (1999) 1658–1660, https://doi.org/10.1126/science.284.5420.1658.

[8] H. Noda, H. Araki, S. Goossens, Y. Ishihara, K. Matsumoto, S. Tazawa, N. Kawano, S. Sasaki, Illumination conditions at the lunar polar regions by KAGUYA(SELENE) laser altimeter, Geophys. Res. Lett. 35 (2008), L24203, https://doi.org/10.1029/2008GL035692.

[9] D.B.J. Bussey, J.A. McGovern, P.D. Spudis, C.D. Neish, H. Noda, Y. Ishihara, S.-A. Sørensen, Illumination conditions of the south pole of the Moon derived using Kaguya topography, Icarus 208 (2010) 558–564, https://doi.org/10.1016/j.icarus.2010.03.028.

[10] E. Mazarico, G.A. Neumann, D.E. Smith, M.T. Zuber, M.H. Torrence, Illumination conditions of the lunar polar regions using LOLA topography, Icarus 211 (2011) 1066–1081, https://doi.org/10.1016/j.icarus.2010.10.030.

[11] D. De Rosa, B. Bussey, J.T. Cahill, T. Lutz, I.A. Crawford, T. Hackwill, S. van Gasselt, G. Neukum, L. Witte, A. McGovern, P.M. Grindrod, J.D. Carpenter, Characterisation of potential landing sites for the European Space Agency's Lunar Lander project, Planet. Space Sci. 74 (2012) 224–246, https://doi.org/10.1016/j.pss.2012.08.002.

[12] P. Gläser, F. Scholten, D. De Rosa, R. Marco Figuera, J. Oberst, E. Mazarico, G. A. Neumann, M.S. Robinson, Illumination conditions at the lunar south pole using high resolution Digital Terrain Models from LOLA, Icarus 243 (2014) 78–90, https://doi.org/10.1016/j.icarus.2014.08.013.

[13] P. Gläser, J. Oberst, G.A. Neumann, E. Mazarico, E.J. Speyerer, M.S. Robinson, Illumination conditions at the lunar poles: implications for future exploration, Planet. Space Sci. 162 (2018) 170–178, https://doi.org/10.1016/j.pss.2017.07.006.

[14] M.K. Barker, E. Mazarico, G.A. Neumann, D.E. Smith, M.T. Zuber, J.W. Head, Improved LOLA elevation maps for south pole landing sites: error estimates and their impact on illumination conditions, Planet. Space Sci. 203 (2021), 105119, https://doi.org/10.1016/j.pss.2020.105119.

[15] Y. Zou, Y. Liu, Y. Jia, Overview of China's upcoming Chang'E series and the scientific objectives and payloads for Chang'E 7 mission, in: 51st Lunar and Planetary Science Conference, 2020, p. 1755. Houston, TX.

[16] M.T. Zuber, J.W. Head, D.E. Smith, G.A. Neumann, E. Mazarico, M.H. Torrence, O. Aharonson, A.R. Tye, C.I. Fassett, M.A. Rosenburg, H.J. Melosh, Constraints on the volatile distribution within Shackleton crater at the lunar south pole, Nature 486 (2012) 378–381, https://doi.org/10.1038/nature11216.

[17] J.R. Arnold, Ice in the lunar polar regions, J. Geophys. Res. 84 (1979) 5659, https://doi.org/10.1029/JB084iB10p05659.

[18] S. Li, P.G. Lucey, R.E. Milliken, P.O. Hayne, E. Fisher, J.-P. Williams, D.M. Hurley, R.C. Elphic, Direct evidence of surface exposed water ice in the lunar polar regions, Proc. Natl. Acad. Sci. U.S.A. 115 (2018) 8907–8912, https://doi.org/10.1073/pnas.1802345115.

[19] L.F.A. Teodoro, V.R. Eke, R.C. Elphic, Spatial distribution of lunar polar hydrogen deposits after KAGUYA (SELENE), Geophys. Res. Lett. 37 (2010), https://doi.org/10.1029/2010GL042889.

[20] A. Colaprete, P. Schultz, J. Heldmann, D. Wooden, M. Shirley, K. Ennico, B. Hermalyn, W. Marshall, A. Ricco, R.C. Elphic, D. Goldstein, D. Summy, G. D. Bart, E. Asphaug, D. Korycansky, D. Landis, L. Sollitt, Detection of water in the LCROSS ejecta plume, Science 330 (2010) 463–468, https://doi.org/10.1126/science.1186986.

[21] D.E. Smith, M.T. Zuber, G.B. Jackson, J.F. Cavanaugh, G.A. Neumann, H. Riris, X. Sun, R.S. Zellar, C. Coltharp, J. Connelly, R.B. Katz, I. Kleyner, P. Liiva, A. Matuszeski, E.M. Mazarico, J.F. McGarry, A.-M. Novo-Gradac, M.N. Ott, C. Peters, L.A. Ramos-Izquierdo, L. Ramsey, D.D. Rowlands, S. Schmidt, V.S. Scott, G.B. Shaw, J.C. Smith, J.-P. Swinski, M.H. Torrence, G. Unger, A.W. Yu, T. W. Zagwodzki, The lunar orbiter laser altimeter investigation on the lunar reconnaissance orbiter mission, Space Sci. Rev. 150 (2010) 209–241, https://doi.org/10.1007/s11214-009-9512-y.

[22] C.H. Acton, Ancillary data services of NASA's navigation and ancillary information facility, Planet. Space Sci. 44 (1996) 65–70, https://doi.org/10.1016/0032-0633(95)00107-7.

[23] J. Flahaut, J. Carpenter, J.-P. Williams, M. Anand, I.A. Crawford, W. van Westrenen, E. Füri, L. Xiao, S. Zhao, Regions of interest (ROI) for future exploration missions to the lunar South Pole, Planet. Space Sci. 180 (2020), 104750, https://doi.org/10.1016/j.pss.2019.104750.

[24] D.A. Paige, M.C. Foote, B.T. Greenhagen, J.T. Schofield, S. Calcutt, A.R. Vasavada, D.J. Preston, F.W. Taylor, C.C. Allen, K.J. Snook, B.M. Jakosky, B.C. Murray, L. A. Soderblom, B. Jau, S. Loring, J. Bulharowski, N.E. Bowles, I.R. Thomas, M. T. Sullivan, C. Avis, E.M. De Jong, W. Hartford, D.J. McCleese, The lunar reconnaissance orbiter diviner lunar radiometer experiment, Space Sci. Rev. 150 (2010) 125–160, https://doi.org/10.1007/s11214-009-9529-2.

[25] N. Schorghofer, Mars: quantitative evaluation of crocus melting behind boulders, APJ (Acta Pathol. Jpn.) 890 (2020) 49, https://doi.org/10.3847/1538-4357/ab612f.

[26] N. Schorghofer, O. Aharonson, The lunar thermal ice pump, APJ (Acta Pathol. Jpn.) 788 (2014) 169, https://doi.org/10.1088/0004-637X/788/2/169.

[27] N. Schorghofer, J.-P. Williams, Mapping of ice storage processes on the Moon with time-dependent temperatures, Planet. Sci. J. 1 (2020) 54, https://doi.org/10.3847/PSJ/abb6ff.

[28] K. Zacny, P. Chu, G. Paulsen, A. Avanesyan, J. Craft, L. Osborne, Mobile in-situ water extractor (MISWE) for mars, Moon, and asteroids in situ resource utilization, in: AIAA SPACE 2012 Conference & Exposition, American Institute of Aeronautics and Astronautics, Pasadena, California, 2012, https://doi.org/10.2514/6.2012-5168.